Chapter

Aerocapture, Aerobraking, and Entry for Robotic and Human Mars Missions

Ye Lu

Abstract

This chapter provides an overview of the aeroassist technologies and performances for Mars missions. We review the current state-of-the-art aeroassist technologies for Mars explorations, including aerocapture, aerobraking, and entry. Then we present a parametric analysis considering key design parameters such as interplanetary trajectory and vehicle design parameters (lift-to-drag ratio, ballistic coefficient, peak g-load, peak heat rate, and total heat load) for aerocapture, aerobraking, and entry. A new perspective on a rapid aerobraking concept will be provided. The analysis will include first-order estimates for thermal loading, thermal protection systems material selection, and vehicle design. Results and discussion focus on both robotic missions and human missions as landed assets and orbiters.

Keywords: aerocapture, aerobraking, entry, robotic mission, human mission

1. Introduction

Aeroassist maneuvers are a family of maneuvers that use aerodynamic forces to change a spacecraft orbit and they include atmospheric entry, aerocapture, aerobraking, and aerogravity-assist. Atmospheric entry is used for in situ explorations, both for robotic and human missions. Atmospheric entry at Mars has been attempted many times by multiple space agencies. Entry at Mars was considered a challenging task mainly due to the unique atmospheric structure [1]. The atmosphere is substantial that aerothermodynamic heating is a consideration, yet the atmosphere is very thin that the aerodynamic drag is barely enough for entry vehicles to decelerate to a velocity at high altitude to safely initiate the final descent stage for a soft landing (i.e., parachute or retro-propulsion).

The concept of using atmosphere to change orbit can be traced back to the earliest publication by London in 1961 [2], which later evolved intro three main categories—aerobraking, aerocapture, and aerogravity-assist. Aerobraking is a maneuver where spacecraft uses atmospheric drag to reduce its orbital period, and it can be used for orbit transfer vehicles from GEO to LEO, or after initial orbit insertion for planetary missions. In the context of Mars missions, aerobraking maneuver is considered free in terms of system requirement because no additional system/mass is needed to perform the maneuver. All the prior aerobraking spacecraft use solar panel as the drag device to decelerate. However, aerobraking

maneuver is not free in terms of operational cost. Due to the long duration of aerobraking maneuver—on the order of months, constant ground operation is required in the past for aerobraking maneuver, which requires hours of staffs and dedicated time with the Deep Space Network (DSN) for position tracking [3].

Aerocapture is an orbit insertion maneuver. Upon first approaching a planet upon hyperbolic trajectory, the spacecraft passes the body's atmosphere once to decelerate and achieve a captured orbit after the single pass. Aerocapture maneuver has been studied in the literature but has never been tested or demonstrated in flight. Aerocapture at Mars is considered side-by-side with aerobraking or direct propulsive orbit insertion.

Aerogravity-assist is a maneuver for interplanetary transfer and most often considered for fast transfer time to the outer solar system for which Mars can be used as a destination to perform aerogravity-assist maneuver, therefore aerogravity-assist will not be discussed in detail in this chapter.

The structure of the chapter is as follows: in Section 2 we discuss the mathematical models and summarize the key parameters for aeroassist maneuvers and vehicles. In Section 3, aerobraking technology is presented along with a new perspective on aerobraking at Mars. In Section 4, we discuss Mars entry technology and the system performance and requirements for future missions. In Section 5, we discuss the performance and system requirements for aerocapture.

2. Mathematical models

2.1 Equations of motion

Assuming a nonrotating body in the body-centered and body-fixed reference frame, the equations of motions for entry, aerocapture, and aerobraking are as follows [4]:

$$\dot{\theta} = \frac{V \cos\gamma \cos\chi}{r \cos\phi} \tag{1}$$

$$\dot{\phi} = -\frac{V \cos\gamma \sin\chi}{r} \tag{2}$$

$$\dot{r} = V \sin\gamma \tag{3}$$

$$\dot{V} = -\frac{q}{\beta} - g \sin\gamma \tag{4}$$

$$\dot{\gamma} = -\frac{q(L/D)}{V\beta} \cos\sigma + \left(\frac{V}{r} - \frac{g}{V}\right) \cos\gamma \tag{5}$$

$$\dot{\chi} = \frac{q(L/D)}{V\beta} \frac{\cos\sigma}{\cos\gamma} + \frac{V}{r} \cos\gamma \sin\chi \tan\phi + \frac{g}{V} \frac{\cos\chi}{\cos\gamma} \tag{6}$$

where θ and ϕ are the longitude and latitude in a spherical surface model; r the radial distance from the center; χ is the heading angle measured clockwise from the direction of local parallel; V is the velocity of the vehicle; γ is the flight path angle (positive above local horizon); σ is the bank angle, which is the rotation angle about the relative velocity vector; $\beta = m/(C_D A)$ is the ballistic coefficient where m is the vehicle mass and C_D is the aerodynamic drag coefficient; and $q = (1/2)\rho V^2$ is the dynamic pressure, where ρ is the density of the atmosphere, and L and D are the lift and drag forces respectively and are defined as:

$$L = \frac{1}{2}\rho V^2 A C_L, \qquad D = \frac{1}{2}\rho V^2 A C_D \tag{7}$$

where C_L is the aerodynamic lift coefficient, and A is the aerodynamic reference area of the vehicle. The angle of attack, α, affects the value of C_L and C_D, and is assumed constant as the trim angle of attack. $g = \mu/r^2$ is the radial component of the gravitational acceleration.

These equations of motion are used throughout this chapter for numerical analysis of trajectories during atmospheric fly-through or entry.

2.2 Aerothermodynamic heating

As the spacecraft flies through the atmosphere at hypersonic speed, the aerothermodynamic heating can be substantial for entry and aerocapture. Aerothermodynamic heating consists of mainly two types of dominating heat transfers: convective and radiative. Sutton and Graves [5] developed an empirical relation for convective heat rate with an arbitrary gas mixture:

$$\dot{q}_c = k(\rho/R_n)^{0.5} V^3 \tag{8}$$

where R_n is the nose radius in m. $\dot{q}_c$ has the unit of W/cm^2 and k has a value of 1.8980×10^{-8}, ρ is the atmospheric density. The empirical relation for radiative heating rate, $\dot{q}_r$ is W/cm^2 follows [6]:

$$\dot{q}_r = 2.35 \times 10^4 r_n^{0.526} \rho^{1.19} f(V) \tag{9}$$

where $f(V)$ is provided for velocities between 6000 m/s and 9000 m/s and is shown in **Figure 1**. At low speed, radiative heating becomes insignificant due to $f(V)$ approaching zero.

2.3 Vehicle designs

Thermal protection system (TPS) is an important vehicle component for all aeroassist maneuvers to protect the spacecraft from the heat generated during the atmospheric pass. Entry and aerocapture can share the vehicle designs as both maneuvers result in very high heat, which warrants TPS. However, aerobraking maneuvers have been achieved without a dedicated TPS and solar panels had been used as the drag device to reduce orbital period; therefore, the following discussion

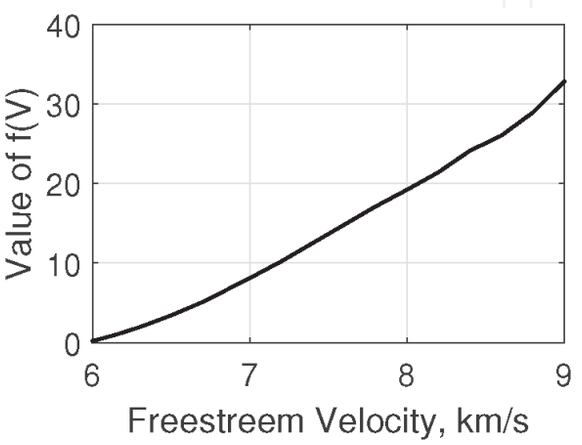

Figure 1.
Coefficient value $f(V)$ as a function of velocity for radiative heating relation [6].

on vehicle designs is applicable to aerocapture and entry. Heritage blunt-body rigid aeroshell designs have been proven for both robotic and manned missions. Most robotic missions used ballistic entry vehicles, which have no active guidance or control (e.g., Mars Pathfinder, Mars Exploration Rovers (MER), and Mars Phoenix), whereas lifting body entry vehicles are used for manned missions and some Mars missions; for example, Mars Science Laboratory used a lifting vehicle in order to meet the landing accuracy requirement and Apollo entry capsules met the safe g-load limit acceptable to humans.

With lifting vehicle design, the guidance and control actively modulate the direction of the lift vector thus to control the trajectory, which is also called bank modulation. The lifting vehicles are typically designed with a nominal L/D with center-of-mass offset or asymmetric heatshield, and are also equipped with thrusters to control the orientation of the lifting vector. **Table 1** lists some lifting body entry vehicles. Vehicle design with spherical section and sphere-cones are most popular and have been used for all entry missions and they can provide L/D of more than 0.3. These rigid body aeroshells are shown feasible for both entry and aerocapture missions for various planetary bodies [8–10].

Adaptable Deployable Entry and Placement Technology (ADEPT) [11] and Hypersonic Inflatable Aerodynamic Decelerator (HIAD) [12] are deployable entry systems that are currently being developed. Both ADEPT and HIAD are applicable to a range of mission sizes from small satellites to larger payloads. Ellipsled vehicle design, or mid-L/D vehicle, has been proposed as a means to increase vehicle control authority (e.g., for ice giants missions [8]) or deliver higher payload mass, such as for human Mars architectures. Starbody waverider can achieve higher nominal L/D (>5.0) than other designs and is mostly useful for interplanetary transfer maneuvers such as aerogravity-assist; therefore, it is only referenced here for comparison [7, 13]. Higher L/D vehicles are available, but in the context of Mars missions, they have very limited applications.

Drag modulation, in addition to bank modulation, is another design that provides the vehicle control authority. Drag modulation uses ballistic vehicles but with additional drag skirt that can be modified to change the vehicle's ballistic coefficient, thus achieving trajectory control in the atmosphere. Such vehicles would require a large ratio for the designed low and high values of ballistic coefficients. Drag modulations can be used for both entry and aerocapture at Mars [14, 15].

Angle-of-attack modulation has also been investigated for Mars entry [16] and shown feasible for aerocapture missions [17]. Direct force control is yet another control mode for entry vehicles, which uses active flaps to create moments and controls the angle-of-attack and side slip angles [18]. Both of the control modes

Vehicle design	Planet	Mission (year)	Entry mass, kg	$(L/D)_{trim}$
Spherical section	Earth	Apollo (1960s)	5560	>0.30
Sphere-cone	Mars	Viking I and II (1976)	576	0.18
Sphere-cone	Mars	MSL (2012)	3380	0.24
ADEPT/HIAD	—	—	Variable	~0.2
Ellipsled	Neptune	—	~6000	0.6–0.8
—	Earth	Space Shuttle	~100,000	1 (hypersonic)
Starbody Waverider	—	Aeroassist	~100,00	~2 [7]

Table 1.
Performance and spacecraft parameters for past Venus and Mars missions using aerobraking.

require a high accuracy in hypersonic flow modeling and the uncertainties at hypersonic speed can be very difficult to predict; therefore, they have mostly been studied in paper and has not been implemented in missions.

Magnetohydrodynamics flow control is another means to actively control the trajectory, which uses the Lorentz force (i.e., the interaction between the plasma field from the hypersonic entry and magnetic field) [19]. It has been shown useful for entry trajectory control and similar is applicable for aerocapture trajectory control. Last but not the least is applying propulsion during aerocapture maneuver to create propulsive "lift" force in order to achieve the necessary trajectory control [20].

3. Aerobraking at Mars

Aerobraking maneuver was first successfully demonstrated at Venus with Magellan mission in 1993 after completing its prime mission. Magellan used aerobraking maneuver to reduce its orbital period from 3.23 h to 1.57 h. Following the Magellan's success, three Mars missions have used aerobraking as an enabling technology to reduce the propellant requirement to enter the target science orbits. The three missions are Mars Global Surveyor (MGS), Mars Odyssey, and Mars Reconnaissance Orbiter (MRO), which were launched in 1996, 2001, and 2005 respectively. **Table 2** summarizes the spacecraft parameters and aerobraking performances for selected aerobraking missions. As shown, the fuel mass saving for all three Mars missions are all over 1000 m/s, which is very significant compared with the launch mass. According to the rocket equation, the propellant mass follows an exponential relation to the required ΔV, the amount of fuel savings can be considered enabling for MGS and Odyssey.

Aerobraking operation includes mainly three phases—walk-in phase, main phase, and walk-out phase. The walk-in phase follows the initial Mars orbit insertion, and reduces the periapsis altitude within Mars atmosphere. During the main phase of aerobraking, the spacecraft uses atmospheric drag to reduce the energy and apoapsis altitude. Past missions have used the solar panel as the main drag device. The

Spacecraft	**Magellan**	**MGS**	**Odyssey**	**MRO**
Destination	Venus	Mars	Mars	Mars
Launch mass, kg	360	1060	725	2180
Propellant mass, kg	2414	385	348.7	1149
Payload mass, kg	154	78	44.5	139
AB ΔV saving, m/s	1220	1220	1090	1190
AB fuel saving, kg	490	330	320	580
AB duration	70 days	6 months	2.5 months	5 months
Period before AB, h	3.2	45	18	34
Period after AB, h	1.6	1.9	2	1.9
AB periapsis range, km	171.3–196.9	100–149	107–119	97–110
Dynamic pressure, N/m^2	0.2–0.3	0.6[a]	0.2–0.3	—
Heat rate, W/cm^2	—	—	—	0.75–1.6

[a] *Dynamic pressure is reduced to 0.2 N/m^2 after the failure of solar panel hinge.*

Table 2.
Performance and spacecraft parameters for past Venus and Mars missions using aerobraking.

dynamic pressure, heat rate, or temperature on the solar panel are monitored to ensure the integrity of the solar panel. During the main phase, constant ground operations are needed in order to actively control the periapsis altitude via minor apoapsis burns so that the solar panel will not overheat. Over a course of months and after hundreds of atmospheric passes, the target apoapsis altitude will be achieved. The walk-out phase is simply a series of impulsive burns at the apoapsis to raise the periapsis altitude out of the atmosphere and to the target science orbit.

3.1 Aerobraking maneuver constraints

The primary constraints of aerobraking maneuver are the structural load and maximum temperature of the solar panel (or drag panel in general). As the spacecraft flies through the upper atmosphere, aerodynamic drags generate heat and increase the temperature of the solar panel. In addition, the drag forces exert structural load on the vehicle, in particular the hinges where the solar panel is connected to the main structure. Most spacecraft use deployable solar panels due to the volume restriction during launch; thus, the connector hinges of the solar panel are usually deployable. One measure of the structural load is the dynamic pressure at periapsis, which is also the maximum dynamic pressure. It is also found that maximum temperature on the solar panel is correlated with the dynamic pressure at periapsis. **Table 2** summarizes the constraints for dynamic pressure and heat rate of the previous aerobraking missions. Magellan, MGS, and Mars Odyssey all used dynamic pressure at periapsis as the constraint metric while MRO used heat rate as the measure of constraint. These values have been flight-tested and proven to be acceptable using only solar panels as the drag device.

3.2 Aerobraking with dedicated structure

Aerobraking maneuver has been considered "free" in terms of the mass budget for spacecraft and it has saved thousands of kilograms of propellant for the past missions as shown in **Table 2**. However, aerobraking maneuvers usually take months. It may be acceptable for robotics missions, but for human missions, spending several more months to perform aerobraking to save propellant mass may be prohibitive.

A novel way for faster aerobraking maneuver is by diving deeper in the atmosphere to achieve more deceleration from a single atmospheric pass, thus reducing the time required to perform the aerobraking maneuver. Dedicated aerobraking hardware using deployable structure and membrane has been investigated in Ref. [21] but with a similar heat rate and dynamic pressure as from the solar panels. With a lightweight deployable structure, the effective drag area is increased and higher deceleration can be achieved from every atmospheric pass.

Ballistic coefficient β in Eqs. (1)–(6) is an important parameter that relates the vehicle mass and the effective aerodynamic drag area. With all things equal, a larger drag area results in a lower ballistic coefficient while a heavier vehicle results in a higher ballistic coefficient. For robotic missions, the ballistic coefficients are usually in the range of 50–150 kg/m^2, whereas for human missions, high ballistic coefficients ($\sim$1000 kg/m^2) can be expected.

3.3 Aerobraking design trade

To evaluate the performance of aerobraking maneuver, a numerical analysis is conducted to obtain the key metrics, such as the dynamic pressure, peak heat rate, and effective ΔV. A range of vacant periapsis altitudes are assessed for the entire

range of entry velocities, 3.49–4.93 km/s (i.e., velocity of a 129-km circular orbit and the escape velocity at entry altitude of 129 km). Different entry velocities and vacant periapsis altitudes result in different dynamic pressure, peak heat rate, and effective ΔV, which are shown as contours in **Figure 2**. It is important to note that the lower left area where the contours end corresponds to crash trajectories; that is, the vacant periapsis altitude is too low and the vehicle will enter the atmosphere entirely. For aerobraking, that is the restricting region.

While **Figure 2** shows the general trends of the design parameters, it only contains limited information to design aerobraking maneuver with a dedicated hardware. One parameter that is of the least interest is the vacant periapsis altitude. After every atmospheric pass, a very small correction ΔV is executed at apoapsis point in order to adjust the vacant periapsis altitude. Thus, vacant periapsis altitude can be adjusted during flight. By replacing the vacant periapsis with ΔV, and plotting the same metrics, such as dynamic pressure and peak heat rate on the chart, we obtain **Figure 3**. Note that orbital periods for each entry velocity and ΔV values are also plotted for reference. At a specific entry velocity, each ΔV value corresponds to only one vacant periapsis altitude. Therefore, vacant periapsis altitude is embedded in ΔV and has not been lost.

From **Figure 3**, we can identify the relations between the constraints (i.e., dynamic pressure or heat rate) with the orbital maneuvers. Using a dynamic pressure limit of 0.5 N/m^2, we can track the dynamic pressure contour of 0.5 N/m^2 from the right to the left. As the orbital period decreases, with the same dynamic pressure limit, more ΔV can be achieved at lower velocity. Starting an orbital period of 240 h (10 days), with a limit of 0.5 N/m^2, the initial ΔV per atmospheric pass is about 0.3 m/s per atmospheric pass. If the orbital period is reduced from 240 h to 24 h (i.e., reducing velocity from 4.88 km/s to 4.71 km/s), it will take approximately 450 atmospheric passes, which is equivalently more than 6 years in duration.

In order to show the effects of ballistic coefficients on aerobraking performance, **Figures 4** and **5** present the design parameters for ballistic coefficients of 50 kg/m^2 and 900 kg/m^2 respectively. By comparison, vehicles with lower ballistic

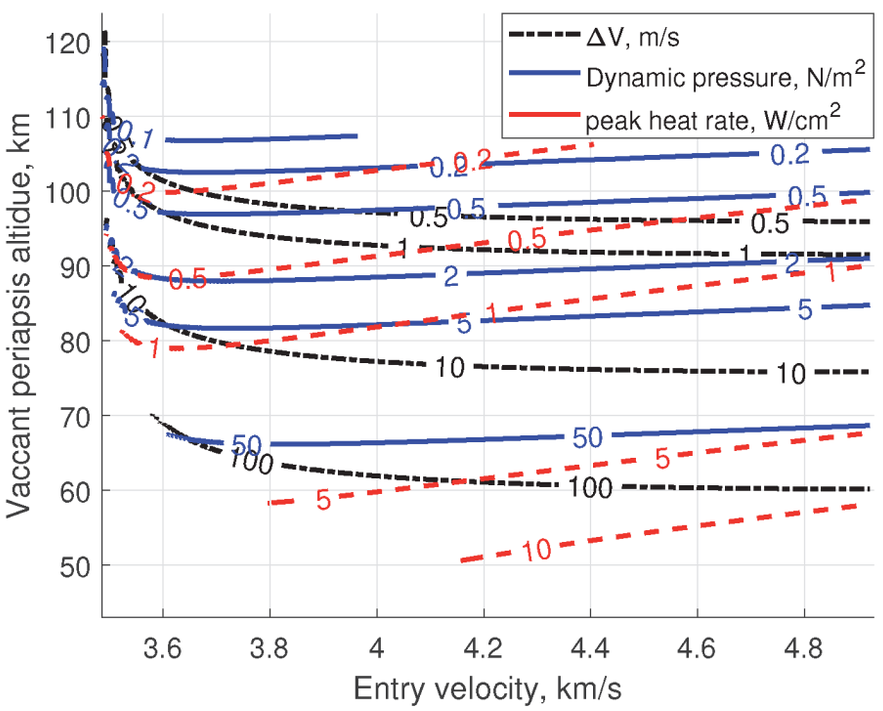

Figure 2.
Performance and design parameters for aerobraking maneuver for vehicle ballistic coefficient of 200 kg/m².

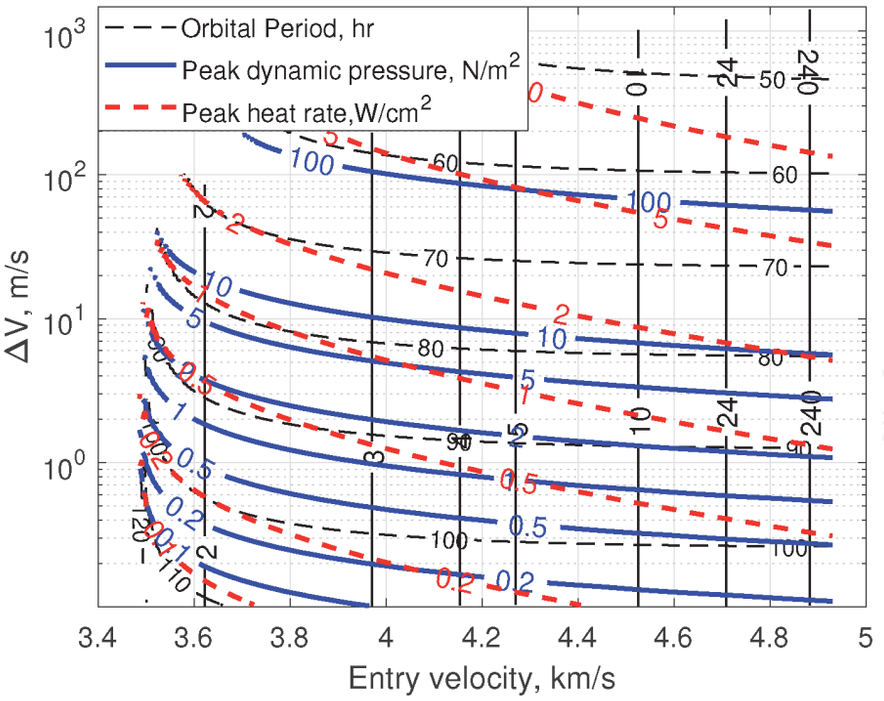

Figure 3.
Performance and design parameters for aerobraking maneuver for vehicle ballistic coefficient of 200 kg/m².

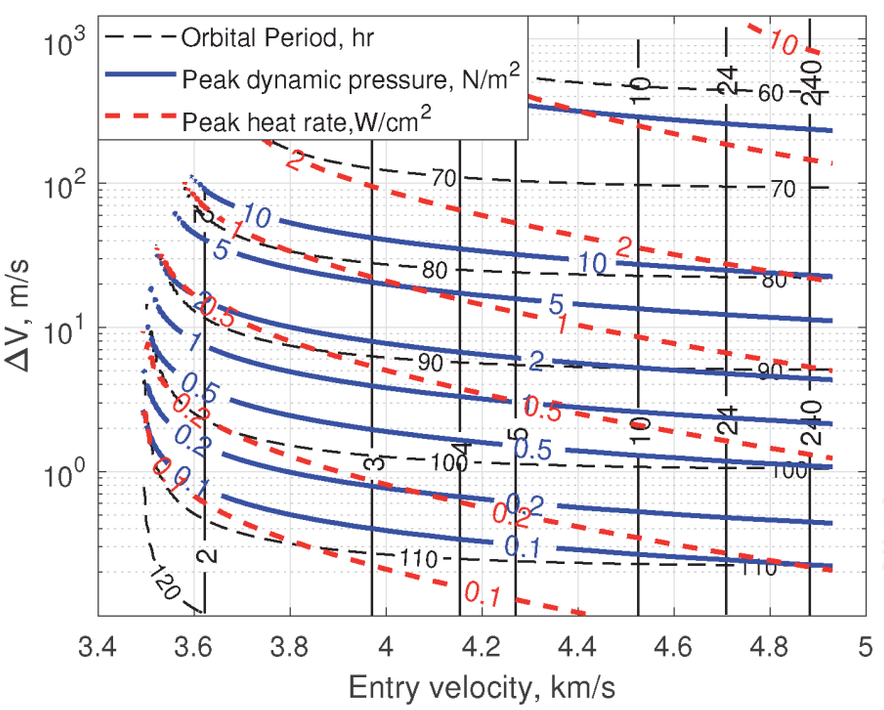

Figure 4.
Performance and design parameters for aerobraking maneuver for vehicle ballistic coefficient of 50 kg/m².

coefficients can decelerate at a higher rate with the same constraints. Considering the same limit of 0.5 N/m^2 for ballistic coefficient of 50 kg/m^2, the ΔV at 240-h period orbit is about 1.3 m/s. A ballistic coefficient of 50 kg/m^2 is roughly the value for the past aerobraking missions, and the duration for aerobraking maneuver to reduce the orbital period from 34 h to 1.9 h (as for MRO) is about 5 months.

For potential human missions using aerobraking, that is, assuming a ballistic coefficient of 900 kg/m^2, the vehicle needs to take a more aggressive approach in terms of the constraints in order to achieve the desired orbit in the same amount of

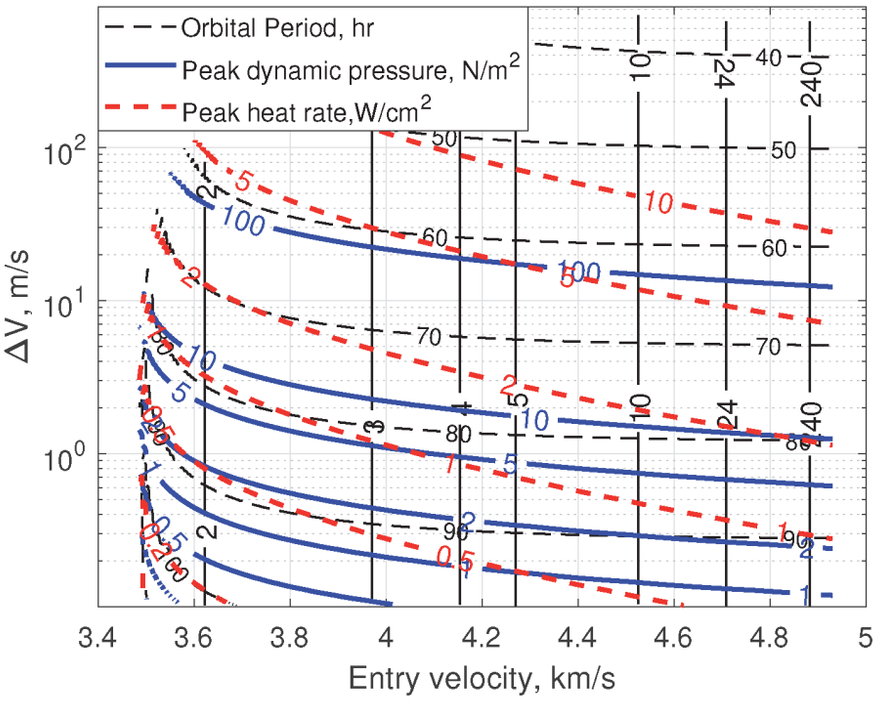

Figure 5.
Performance and design parameters for aerobraking maneuver for vehicle ballistic coefficient of 900 kg/m².

time for vehicles with a lower ballistic coefficient. Using the same timeline (i.e., 6 months) as the past robotic aerobraking missions, human-class missions would require a minimum dynamic pressure limit of 4.5 N/m^2. For faster aerobraking missions, a 1-month aerobraking maneuver requires a dynamic pressure limit of 25 N/m^2; a 10-day aerobraking maneuver requires 75 N/m^2. Note that at higher dynamic pressure, the heat rate constraint may be more dominating, and the numbers are only rough estimates for the purpose of illustrating the application of the plots.

4. Atmospheric entry at Mars

Mars atmospheric entry, descent, and landing are very challenging due to its thin atmosphere [1]. It is difficult for large entry vehicles to achieve enough deceleration for a soft touchdown. Landers and rovers have been successfully delivered to the surface of Mars, but the mass class has been increasing—from 11 kg for Mars Pathfinder, 185 kg for Mars Exploration Rovers, to 900 kg for Mars Curiosity and 1050 kg for Mars 2020. As interests in human Mars missions increase, landing large-size human-rated payload (on the order of 10s of metric ton) on Mars surface becomes important. The main objective of the entry phase is to decelerate the vehicle enough so that the vehicle can reach a low velocity at a high enough altitude for the final descent and landing phase to safely engage. In the following, we will show a parametric analysis for the performance of different vehicle designs, from ballistic vehicles (L/D = 0) to mid-L/D vehicles (L/D up t0 0.8) for human-class missions.

It is important to note that, for robotic missions, the landed mass has been in the range of 100s to 1000s kg, thus with a reasonably large aeroshell (e.g., diameter of 4.5 m), a ballistic coefficient of less than 50 kg/m^2 can be achieved. However, for human-class payloads, there is a need for mid-L/D vehicles, for which the ballistic

coefficients are at least an order of magnitude larger than that of a robotic mission. To conduct the parametric analysis, we use 50 and 900 kg/m^2 as the baseline and show the results corresponding to these vehicle designs. Interested readers are directed to the Mars Design Reference Architecture 5.0 [22] for more details.

4.1 Entry performance parameters

Key performance parameters for atmospheric entry are peak g-load, peak heat rate, and total heat load. Lower values for all the parameters are desired; however, trends for peak heat rate and total heat load are opposite as shown in **Figure 6**. For the same entry velocity, with increase of entry flight-path angles, total heat load decreases whereas peak heat rate and peak g-load increases. As ballistic coefficient increases, an overall increase in all three parameters can be observed.

In **Figure 6**, the black shaded areas in all four plots correspond to exit trajectories, meaning that with the combination of velocity and entry flight-path angle, the vehicle will exit the atmosphere after a short atmospheric flight. Several entry velocities are also worth noting—3.49 km/s is the circular velocity at 129-km altitude, 4.93 km/s for V_∞ of 0 km/s, 7 km/s for V_∞ of 5 km/s, and 9 km/s for V_∞ of 7.5 km/s. A V_∞ of 7.5 km/s is the common maximum value seen for Mars arrival V_∞. Higher arrival velocities are possible but for the purpose of this chapter, an entry velocity of 9 km/s covers a wide range of interplanetary trajectories.

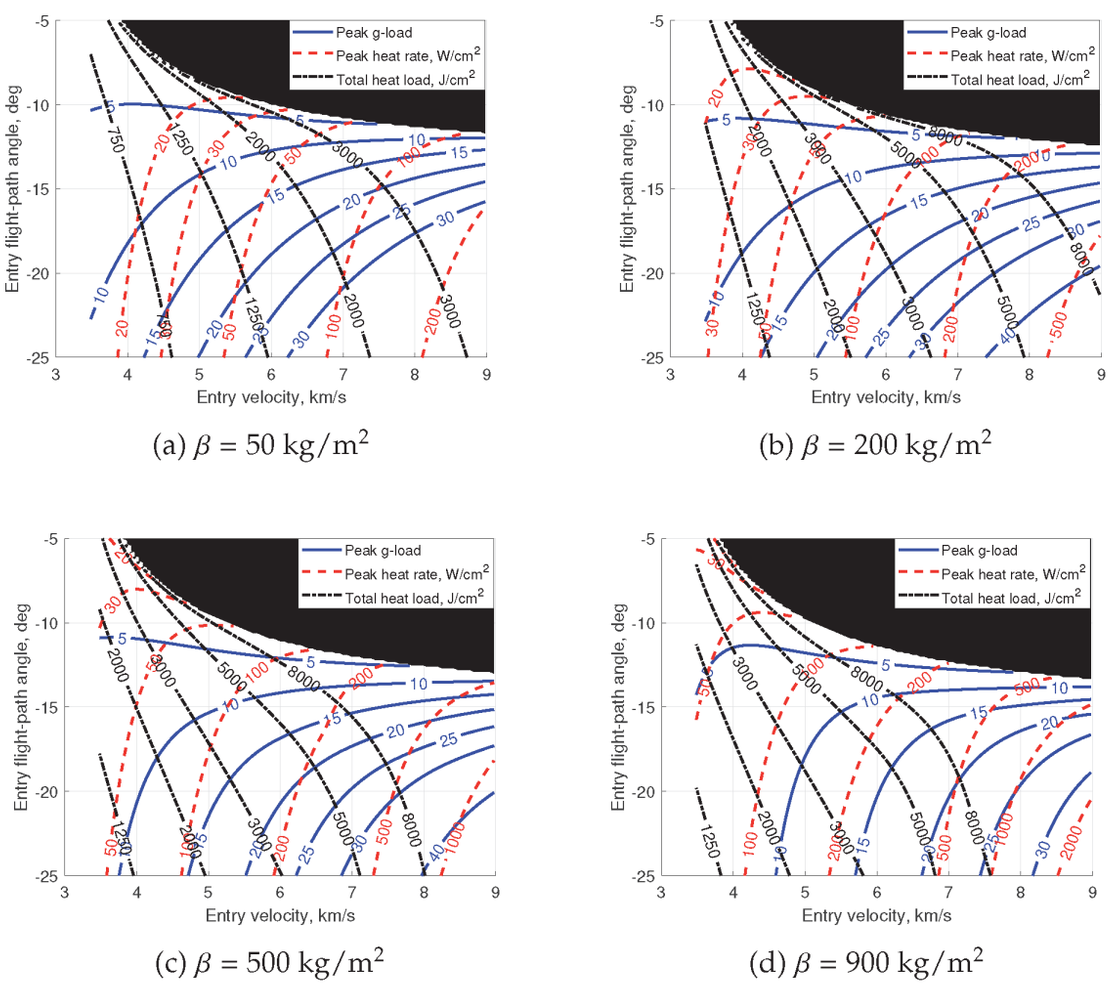

Figure 6.
Entry parameters for ballistic vehicle (L/D = 0), showing peak g-load, peak heat rate, and total heat load for entry velocity from circular speed at 129 km altitude to V_∞ of 7.5 km/s.

At entry flight-path angle of about −11 deg, **Figure 6** shows that the peak g-load only varies slightly with entry velocities, which means that entry at both high arrival velocities and low velocities results in similar g-load at that particular entry flight-path angle. However, the main differences will be the heat rate and heat load. If the mission design allows for a lower arrival velocity, it will decrease both peak heat rate and total heat load.

As a reference for technologies for entry, in particular TPS materials, we have listed some common TPS materials in **Table 3**. Note that heat rate on the order of 100 s W/cm^2 is well within the technology of current TPS material. Phenolic Impregnated Carbon Ablator (PICA) and Heatshield for Extreme Entry Environment Technology (HEEET) are more capable compared with other TPS materials. From **Figure 6**, for robotic missions, that is, ballistic coefficients of 50 and 200 kg/m^2, ACOAT could handle most of the heating conditions.

4.2 Terminal velocity

Terminal velocity at the end of entry phase during an EDL sequence is important for Mars. If the vehicle did not have enough deceleration from the initial entry phase, the descent and landing will not have enough time for execution, eventually leading to a crash. Successful Mars missions all use parachute as a means for descent. **Table 4** lists the altitudes and Mach numbers for the start of final descent phase (i.e., parachute deployment). Note that, each mission delivered the probe to a different altitude on Mars; while the requirements can be different for each mission, the numbers in **Table 4** provide a guideline for the desired mach numbers at the end of the entry phase.

Parachute is not the only means for descent, as high-mass class vehicles are emerging for human missions, the feasibility of a large enough parachute for descending 10s metric tons of payloads are questionable. For such reason,

Material	Density, g/cm^3	Maximum $\dot{q}_s$, W/cm^2	Pressure, atm
Shuttle tiles	0.192–0.352	44	
SRAM family	0.224–0.32	~100	~1
TUFROC	Varies	~300	—
SLA-561V	0.256	100–200	<0.3
AVCOAT		~900	~1
PICA	0.256	>1400	~0.3
HEEET	0.3–1.4	~7000 (tested [24])	—

Table 3.
Properties and performances of TPS materials [8, 9, 23].

Mission	Mach number	Altitude, km	Landing site elevation, km
1976 Viking 1 & 2	1.1	5.79	−3.5
1997 Pathfinder	1.57	9.4	−2.5
2004 MERs	1.77	7.4	−1.9
2012 Curiosity	2.05	10.0	−1.45

Table 4.
Parachute deployment altitude and Mach number.

supersonic retro-propulsion is an attractive option for high-mass systems [25], which could be activated at Mach 2 and above.

To evaluate the overall performance of the terminal velocity of entry systems, **Figure 7** shows the terminal velocities (at 10 km) for small (50 kg/m^2) and large (900 kg/m^2) ballistic coefficients, corresponding to robotic and human missions respectively. Shallow entry flight-path angles are preferred in order to achieve a lower terminal velocity to ensure a safe descent phase. For ballistic coefficient of 50 kg/m^2, the lowest terminal velocity is about 1.7 km/s. The contour line denoting "1.8" in **Figure 7a** shows that the same terminal velocity can be achieved at two different entry flight-path angles. Such phenomena are due to a partial equilibrium glide phase, which is shown in **Figure 8**. The difference between the two trajectories is the downrange, which can be problematic, because any uncertainties in entry condition, atmospheric densities, or aerodynamic properties will cause the vehicle to deviate from the planned trajectory.

For practical design consideration, if pinpoint landing is required, lifting body vehicle is a must in order to actively control the trajectory to the target areas. Mars Science Laboratory is an example where it has a targeted landing site for scientific

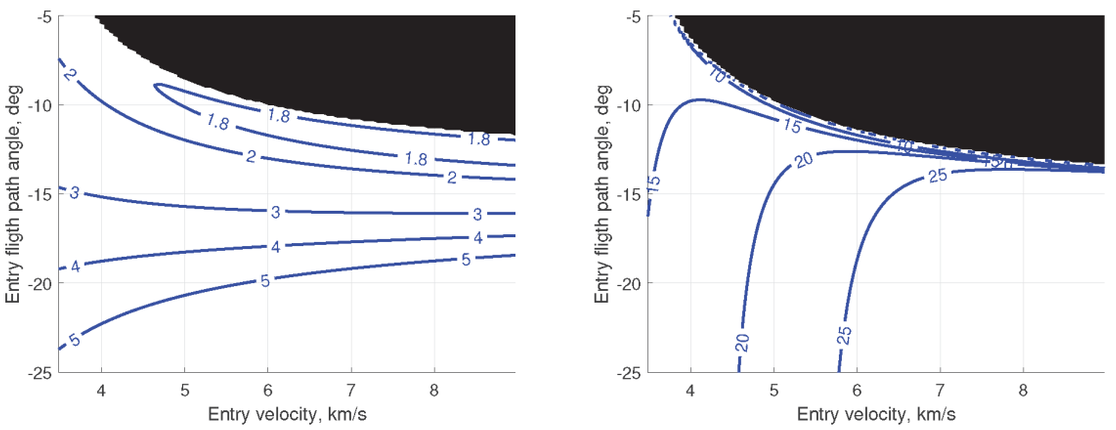

(a) $\beta = 50$ kg/m^2 (b) $\beta = 900$ kg/m^2

Figure 7.
Terminal velocities in Mach number for ballistic vehicle (L/D = 0) at an altitude of 10 km.

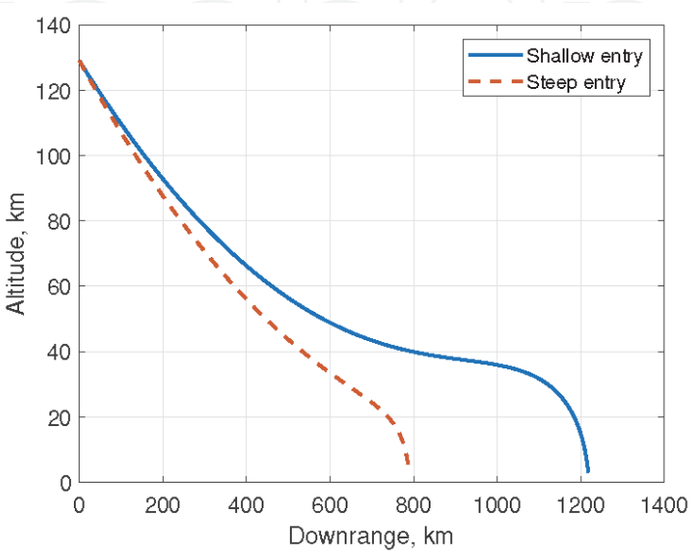

Figure 8.
Ballistic entry trajectories with the same terminal velocity for shallow and steep entry.

explorations. The same landing requirement will also apply for human missions due to the requirement of landing close to the base locations. A guided entry becomes ever important so that at the end of entry phase the vehicle can be within the targeted landing site and with the delivery range of the final descent stage. **Figure 9** shows that adding lifting capability can significantly reduce the terminal velocity compared with **Figure 7a**. For any targeted entry flight-path angles, the terminal velocity at 10 km ranges from Mach 1.3 to 1.5. A vehicle with higher L/D could achieve even lower terminal velocity. The catch however is that, most of these trajectories would leverage the lifting capability to fly higher in altitude to achieve more deceleration.

Shown in **Figure 10** are the trajectory profiles for the same terminal velocity at different entry flight-path angles. A portion of the trajectory skip up thus results in more deceleration. Note that **Figures 9** and **10** are for fully lift-up trajectories only, no guidance has been implemented. The results show that adding lifting capability

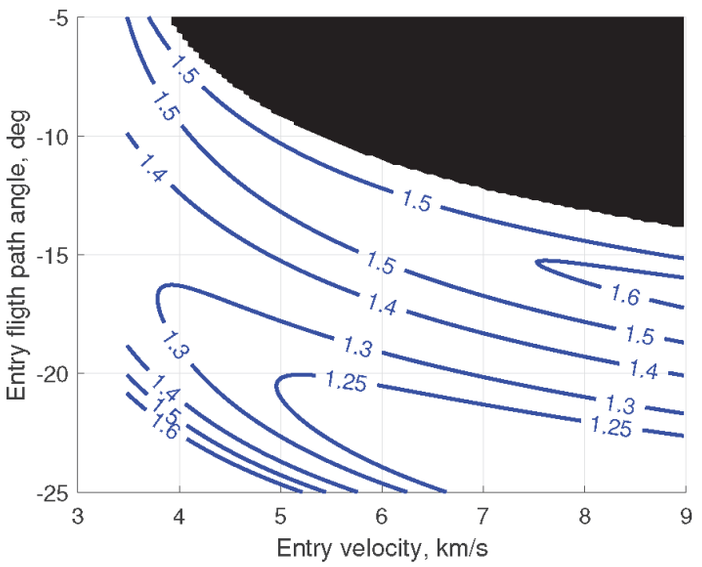

Figure 9.
Terminal velocities in Mach number for vehicle L/D of 0.2 at an altitude of 10 km, β = 50 kg/m^2.

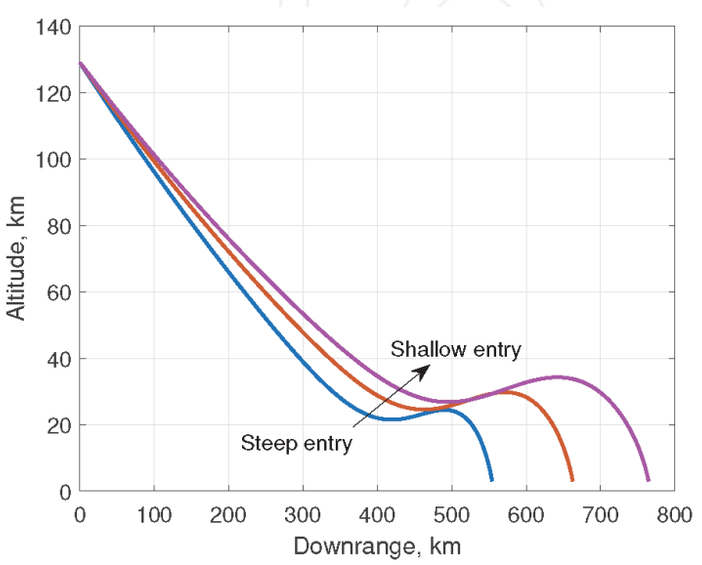

Figure 10.
Trajectory profiles for the same terminal velocity at different entry flight-path angles, using vehicle L/D of 0.2.

can significantly reduce the terminal velocities. Vehicles with higher L/D can achieve even lower terminal velocity due to increased control authority.

5. Aerocapture at Mars

Mars aerocapture has been popular for both small satellite missions and human missions. For small satellite missions, due to the limited mass budget, propulsion system has propellant mass requirement that is too restrictive, and traditional bank modulation requires very complicated thrusters for banking maneuver. Drag modoluation aerocapture has been considered for Mars small satellite missions [26]. Methods for comparing aerocapture with traditional propulsive options and aerobraking were also investigated for Venus in Ref. [27]. For human Mars missions, repeated Mars orbit insertion maneuvers warrant the use of aerocapture to save propellant in order to deliver assets to Mars orbit.

Since aerocapture is an orbit insertion maneuver, the atmospheric entry velocities correspond to V_∞ of 0–7.5 km/s, which is similar to the velocity ranges used for entry, but with the exclusion of entry velocities for closed orbits (which is also the range of entry velocities used for aerobraking analysis).

Aerocapture maneuver is very sensitive to uncertainties; thus in order to ensure a successful aerocapture maneuver, vehicle control authority is required. A measure of such control authority is termed theoretical corridor width, which is measured in deg. Theoretical corridor width is the difference between the maximum and minimum entry flight-path angles that allow the vehicle to be captured given a set of parameters, including arrival V_∞, vehicle L/D, and ballistic coefficients. Another term of corridor width is the required corridor width, which is a measure of the total uncertainties in deg. The uncertainties mainly include atmospheric density uncertainties, vehicle aerodynamic uncertainties, and arrival uncertainties (i.e., target B-plane and entry flight-path angle).

5.1 Aerocapture feasibility

A framework for assessing aerocapture feasibility has been developed and discussed in detail in Ref. [10, 27, 28] and the results in this section follow the same analysis framework. The key design parameters for aerocapture missions are very similar to those for entry except theoretical corridor width. Peak g-load, peak heat rate, and total heat load are the parameters of interests for aerocapture maneuver. **Figures 11** and **12** combine all the design parameters as contours lines onto a single plot including arrival V_∞ and vehicle L/D.

It is important to recognize the implications of the contours. The solid contour "Corridor width" notes the theoretical corridor width and it has a lower limit, which is the required corridor width. For Mars, the required corridor width is conservatively estimated to be 2 deg. [29]. Given that theoretical corridor width has to be greater than the required corridor width, the area under the solid contour of 2 deg. is the unfeasible region for aerocapture due to the lack of control authority. Then the design parameters—peak g-load, peak heat rate, and total heat load—place upper constraints on the aerocapture feasibility. For example, if the mission requires a maximum g-load of 10 Earth g's for a human mission, then we can tell from the feasibility plot, **Figure 11**, that there exists a maximum arrival V_∞ and that the mission designer should only search for trajectories that result in a lower arrival V_∞ than the limit.

DOI: http://dx.doi.org/10.5772/intechopen.93281

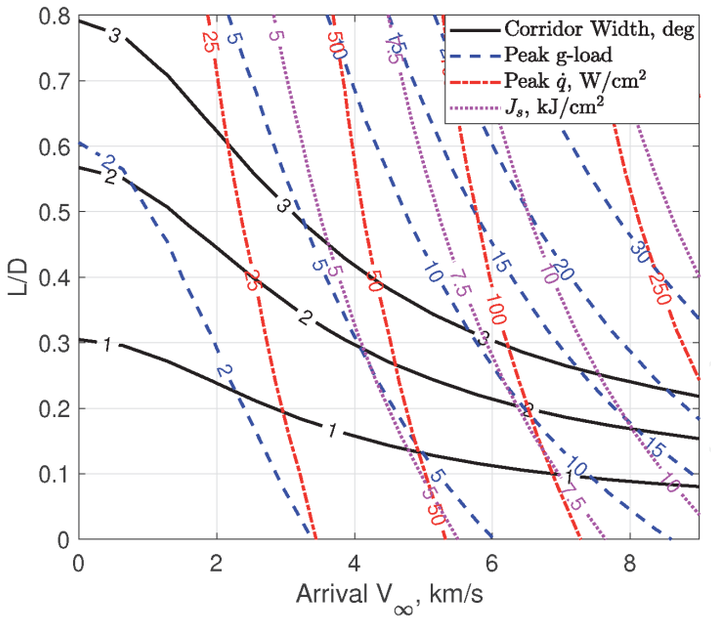

Figure 11.
Aerocapture feasibility plot for $\beta = 50$ kg/m^2.

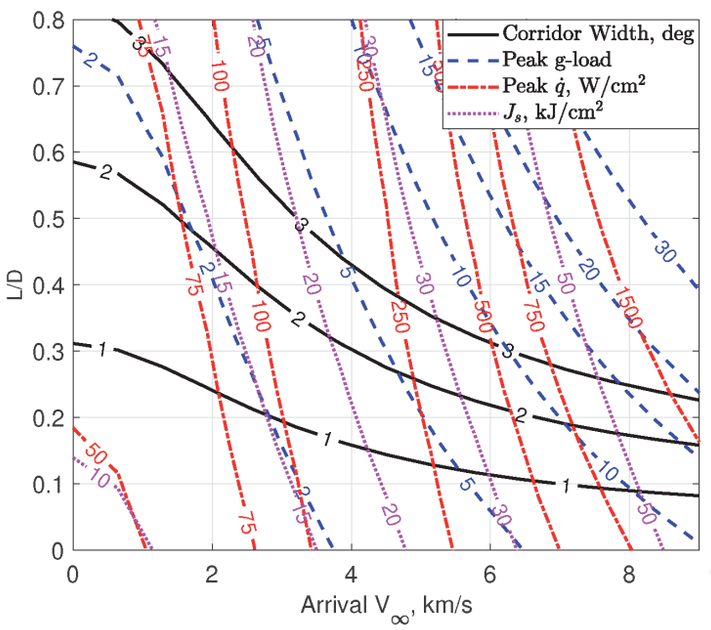

Figure 12.
Aerocapture feasibility plot for $\beta = 900$ kg/m^2.

A common trend of all contours of the design parameters is that they increase with the increase of arrival V_∞ and with increase of vehicle L/D. It is intuitive that higher velocity will result in higher g-load, heat rate, and total heat load. However, the trend for vehicle L/D is due to the assumption used in the analysis that only the worst-case scenarios are used. For a value of vehicle L/D, both full lift-up and full lift-down cases are evaluated and the worse case of the two was recorded and plotted. The design values shown are the worst-case scenarios and it is expected that with guidance and control, the actual values will be lower.

The contours of peak g-load, peak heat rate, and total heat load put constraints on the plots. Similar to how g-load constrains the design feasibility, both peak heat rate and total heat load will constrain the feasible arrival V_∞. As the contour lines of

these design constraints intersect with the theoretical corridor width, there also exists a minimum vehicle L/D for a successful aerocapture. As the constraints become more restrictive (in other words, allowable peak g-load and peak heat rate are reduced), the requirement for vehicle L/D will increase whereas the maximum allowable arrival V_∞ will decrease.

5.2 Aerocapture for robotic and human missions

The difference between **Figures 11** and **12** is the ballistic coefficients. By comparing the two plots, we note that a higher ballistic coefficient results in similar theoretical corridor width (i.e., vehicle control authority), similar peak g-load, but much higher peak heat rate and total heat load. **Figure 11** can be regarded for robotic missions or small satellite missions whereas **Figure 12** for human Mars missions.

Figure 11 shows that the peak heat rate and total heat load are very benign. Even at V_∞ of 9 km/s, the peak heat rates are only around 250 W/cm^2, which is well within the TPS material limits. At lower V_∞, we can even use non-ablative TPS materials such as the tiles used on Space Shuttles as listed in **Table 3**. In terms of peak g-load, robotic missions can usually tolerate a higher g-load than for human missions. The Galileo probe that entered Jupiter's atmosphere was designed to withstand over 200 Earth g's. As a result, in the range of arrival V_∞ considered, the g-load constraints are not too restrictive.

For human Mars missions, as shown in **Figure 12**, the peak heat rates are still well within the current TPS materials. As with higher V_∞ values, peak heat rate can be more challenging. However at around 2000 W/cm^2, HEEET is capable of handling such heat rate. Note that HEEET is an ablative TPS material, which means that it will be difficult to reuse because of the loss of materials. For the purpose of getting humans to Mars, a non-ablative TPS material will be ideal for repeated aerocapture maneuvers. Considering a theoretical corridor width of 2 deg., with a mid-L/D vehicle (L/D of 0.6–0.8), the peak heat rate will be around 75 W/cm^2, which is more than what the shuttle tile can handle. Assuming a non-ablative TPS material can sustain 75 W/cm^2 peak heat rate; then, in **Figure 12**, the area above the contour line of 2 deg. and left of 75 W/cm^2 line is the feasible region for aerocapture, which requires a very low arrival V_∞ of less than 1.5 km/s. In terms of the g-load constraints for human missions, within the areas found, a peak g-load of 2 Earth g's is a very benign condition. It is important to note again, that the worst-case scenarios are shown, and with guidance and control, optimal trajectories can often reduce the peak conditions.

6. Conclusions

In this chapter, a high-level assessment of aerocapture, aerobraking, and entry for robotic and human mission is presented. A comprehensive parametric analysis for all three maneuvers has been investigated while considering the key design parameters. Vehicle aerodynamic properties are key drivers in the performance of these maneuvers. Entry velocities also affect greatly the design parameters. From the results, aerocapture, aerobraking, and entry can be successful for robotic missions, whereas for human Mars missions, there are still challenges that need to be addressed. The challenges are directly related to the risks of the mission, and for human missions, safety is usually the top priority and strategies to mitigate the risk, that is, addressing the challenges will significantly reduce the risk to ensure mission success.

DOI: http://dx.doi.org/10.5772/intechopen.93281

Author details

Ye Lu
Kent State University, Kent, OH, United States

*Address all correspondence to: ylu16@kent.edu

References

[1] Braun RD, Manning RM. Mars exploration entry, descent and landing challenges. Journal of Spacecraft and Rockets. 2007;**44**(2):310-323

[2] London HS. Change of satellite orbit plane by aerodynamic maneuvering. Journal of the Aerospace Sciences. 1962; **29**(3):323-332

[3] Spencer DA, Tolson R. Aerobraking cost and risk decisions. Journal of Spacecraft and Rockets. 2007;**44**(6): 1285-1293

[4] Vinh NX, Busemann A, Culp RD. Hypersonic and Planetary Entry Flight Mechanics. Ann Arbor, MI, USA: The University of Michigan Press; 1980

[5] Sutton K, Graves RA. A general stagnation-point convective-heating equation for arbitrary gas mixtures. In: Technical Report. Hampton, VA, USA: NASA; 1971

[6] Tauber ME, Suttont K, Sutton K. Stagnation-point radiative heating relations for Earth and Mars entries. Journal of Spacecraft and Rockets. 1990; **28**(1):40-42

[7] Knittel JM, Lewis MJ. Concurrent arocapture with orbital plane change using starbody waveriders. The Journal of the Astronautical Sciences. Springer; 2014;**61**(4):319-340

[8] Lockwood MK, Edquist KT, Starr BR, Hollis BR, Hrinda GA, Bailey RW, et al. Aerocapture systems analysis for a Neptune Mission. In: Technical Report. NASA/TM-2006-214300. Hampton, VA, USA: NASA; 2006

[9] Lockwood MK, Queen EM, Way DW, Powell RW, Edquist K, Starr BW, et al. Aerocapture systems analysis for a Titan mission. In: Technical Report NASA/TM-2006-214273. 2006

[10] Lu Y, Saikia SJ. Feasibility assessment of aerocapture for future titan orbiter missions. Journal of Spacecraft and Rockets. 2018;**55**(5): 1125-1135

[11] Venkatapathy E, Arnold J, Fernandez I, Hamm KR, Kinney D, Laub B, et al. Adaptive deployable entry and placement technology (ADEPT): A feasibility study for human missions to Mars. In: 21st AIAA Aerodynamic Decelerator Systems Technology Conference and Seminar, (Dublin, Ireland), AIAA. 2011

[12] Hughes S, Cheatwood F, Dillman R, Calomino A, Wright H, DelCorso J, et al. Hypersonic inflatable aerodynamic decelerator (HIAD) technology development overview. In: 21st AIAA Aerodynamic Decelerator Systems Technology Conference and Seminar, (Dublin, Ireland), AIAA. 2011

[13] Henning GA, Edelman PJ, Longuski JM. Design and optimization of interplanetary aerogravity-assist tours. Journal of Spacecraft and Rockets. 2014;**51**(6):1849-1856

[14] Putnam ZR, Braun RD. Drag-modulation flight-control system options for planetary aerocapture. Journal of Spacecraft and Rockets. 2014; **51**(1):139-150

[15] Putnam ZR, Braun RD. Precision landing at Mars using discrete-event drag modulation. Journal of Spacecraft and Rockets. 2014;**51, 1**:128-138

[16] Lafleur J, Cerimele C. Angle of attack modulation for Mars entry terminal state optimization. In: AIAA Atmospheric Flight Mechanics Conference, Vol. 8, August, Reston, Virigina. American Institute of Aeronautics and Astronautics. 2009. pp. 1-20

[17] Queen EM. Angle-of-attack-modulated terminal point control for Neptune aerocapture. In: 14 AAS/AIAA Space Flight Mechanics Conference, Maui, Hi. AAS. 2004. pp. 04-129

[18] Dwyer Cianciolo A, Powell RW. Entry, descent, and landing guidance and control approaches to satisfy Mars human mission landing criteria. In: AAS/AIAA Flight Mechanics Conference. 2017

[19] Fujino T, Yoshino T, Ishikawa M. Numerical analysis of reentry trajectory coupled with magnetohydrodynamics flow control. Journal of Spacecraft and Rockets. 2008;**45**:911-920

[20] Shibata E. Aeropropcapture: Applying propulsion to aerocapture maneuvers. In: AIAA/AAS Astrodynamics Specialist Conference. 2018

[21] Giersch L, Knarr K, Lyons DT. The dedicated deployable aerobraking structure. In: Technical Report. Pasadena, CA, USA: Jet Propulsion Laboratory; 2011

[22] Drake GG, Yoder GL, McCuistion D, Irvine TB, Radzanowski DP. Human exploration of Mars design reference architecture 5.0. In: Technical Report. Hampton, VA, USA: NASA; 2009

[23] Kolawa E, Balint T, Birur G, Bolotin G, Brandon E, Castillo LD, et al. Extreme environments technologies for future space science missions. In: Technical Report. Pasadena, CA, USA: NASA; 2007

[24] Ellerby D, Gage P, Kazemba C, Mahzari M, Nishioka O, Peterson K, et al. Heatshield for extreme entry environment technology (HEEET) development status. In: 13th International Planetary Probe Workshop, Laurel, MD. 2016

[25] Edquist KT, Desai PN, Schoenenberger M. Aerodynamics for Mars Phoenix entry capsule. Journal of Spacecraft and Rockets. 2011;**48**:713-726

[26] Putnam ZR, Clark IG, Braun RD. Drag modulation flight control for aerocapture. In: IEEE Aerospace Conference. 2012

[27] Girija AP, Lu Y, Saikia SJ. Feasibility and mass-benefit analysis of aerocapture for missions to Venus. Journal of Spacecraft and Rockets. 2020; **57**:58-73

[28] Saikia S, Millane J, Mudek A, Arora A, Witsberger P, Shibata E, et al. Aerocapture assessment at Uranus and Neptune for NASA's ice giant studies. In: Technical Report, PU-AAC-2016-MC-0002. West Lafayette, IN: Purdue University; 2016

[29] Wright HS, Oh DY, Westhelle CH, Fisher JL, Edquist KT, Brown JL, et al. Mars aerocapture systems study. In: Technical Report, NASA/TM-2006-214522 Mars. 2006